Journal of Catalysis 268 (2009) 39–48

Contents lists available at ScienceDirect

Journal of Catalysis

journal homepage: www.elsevier.com/locate/jcat

Spectroscopic study of the electronic interactions in Ru/TiO_2 HDS catalysts

Perla Castillo-Villalón, Jorge Ramírez *

UNICAT, Departamento de Ingeniería Química, Facultad de Química, Universidad Nacional Autónoma de México, Cd. Universitaria, México, D.F. 04510, Mexico

ARTICLE INFO

Article history:
Received 30 June 2009
Revised 27 August 2009
Accepted 29 August 2009
Available online 2 October 2009

Keywords:
Ru/TiO_2 HDS catalysts
Ruthenium sulfide
Thiophene
DBT and 4,6-DMDBT hydrodesulfurization
EPR
UV–Visible–NIR

ABSTRACT

The characteristics of Ru/TiO_2 catalysts sulfided at temperatures from 573 to 873 K were studied by TPR-S, XRD, electron microscopy, EPR, and UV–Visible–NIR. It was found that the structure of the ruthenium sulfided phase formed at the different sulfidation temperatures is essentially the same when supported on alumina or titania. However, when supported on titania effects arising from electronic transfers between the Ru species and the TiO_2 support affect the performance of the catalyst. The high HDS activity of Ru/TiO_2 sulfided at 573 K was explained through the electronic interaction between metallic Ru (coming from the partial reduction of RuS_2) and titania. The low HDS activity of Ru/TiO_2 sulfided at 873 K was explained by the alteration of the already optimum electronic configuration of ruthenium sulfide caused by electron density supplied by the titania support. This provides experimental evidence to support the reported theoretical correlations between electronic structure and HDS activity.

1. Introduction

Studies on the activity of transition metal sulfides (TMS) in the dibenzothiophene hydrodesulfurization (HDS) reaction revealed that the HDS activity of sulfides of the second and third rows is higher than that of sulfides of the first row. A maximum in activity was found for Ru and Os sulfides in the second and third rows, respectively [1]. Similar results were found with other sulfur-containing molecules such as thiophene and 4,6-dimethyl-dibenzothiophene [2–4]. It was proposed that the HDS activity was related to the number of *d* electrons in the HOMO of the TMS. The proposal was based on theoretical calculations that indicated that in the best catalysts the TMS should have the HOMO filled with as many electrons as possible, with t_{2g} instead of e_g character [5–9]. From this point of view, it is not surprising that RuS_2 was the most active HDS catalyst since ruthenium has a HOMO with t_{2g} nature filled with 6 electrons. The importance of the electron population in *d* orbitals in TMS is corroborated by the fact that electronic transfer toward the TMS enhances its HDS activity. An example is the increase in activity experienced by Mo in CoMoS or NiMoS catalytic systems, in which the Co or Ni promoter transfers electronic density to Mo. This behavior helped to define the promoter effect as the capacity to inject electronic density into the *d* orbitals of the TMS [10,11].

The electronic density may also arrive to the TMS coming from supports such as titania, and in that sense titania can be defined as a promoter. It is well documented that the use of titania as a support enhances the HDS activity of TMS such as MoS_2 and WS_2 not only by improving the sulfidation and/or dispersion of the active phase but also by transferring electronic density toward the TMS [12–18]. The possible electronic interaction between titania, which is able to donate electronic density, and RuS_2, which already has the optimum configuration with 6 electrons at the t_{2g} HOMO, is clearly of great interest since it may help to better understand the role of *d* electrons in the HDS activity of TMS.

Supported ruthenium sulfide has particularities that have to be taken into account in the study of Ru/TiO_2 sulfided catalysts. In a recent paper [19] we showed that the sulfidation of Ru/Al_2O_3 catalysts with $H_2S(15\%)/N_2$ at temperatures between 573 and 973 K produces a well-sulfided ruthenium phase (with S/Ru > 2), which contains crystallized ruthenium sulfide (RuS_2-pyrite) and highly defective ruthenium sulfide (RuS_2-amorphous). The relative proportion of the two phases was related to the sulfidation temperature: as the temperature increased more RuS_2-pyrite was formed in detriment of RuS_2-amorphous. For Ru/Al_2O_3 catalysts, at high sulfidation temperature (973 K) practically all the supported ruthenium is transformed into RuS_2-pyrite and the catalyst displays high HDS activity [19]. Amorphous ruthenium sulfide is not stable and undergoes reduction during the HDS reaction while RuS_2-pyrite remains unaltered and is responsible for the HDS activity. Due to the reduction of amorphous ruthenium sulfide, the S/Ru ratio of the catalyst after HDS reaction varies with sulfidation temperature going from S/Ru ~ 1 at low sulfidation temperature (573 K) to S/Ru ~ 2 at high sulfidation temperature (973 K), in accordance with the increasing amount of RuS_2-pyrite in the

* Corresponding author. Fax: +52 55 56 22 53 66.
E-mail addresses: perla@unam.mx (P. Castillo-Villalón), jrs@unam.mx (J. Ramírez).

0021-9517/$ - see front matter © 2009 Elsevier Inc. All rights reserved.
doi:10.1016/j.jcat.2009.08.014

catalyst. This means that the HDS activity of Ru/Al_2O_3 catalysts increases with the sulfur content of the active phase during reaction (higher S/Ru ratio) [19].

It is most likely that the HDS activity of ruthenium sulfide will be affected by the use of a semiconductor support such as TiO_2, although this case has not been studied in the past.

The objectives of the present work are to (a) establish the characteristics and catalytic behavior of ruthenium sulfide particles supported on a semiconductor oxide such as TiO_2; (b) identify the type of electronic interactions between TiO_2 and the supported ruthenium sulfided phase; and (c) determine the consequences of the electronic interactions on the HDS activity of the catalysts. To this end, Ru/TiO_2 catalysts sulfided at different temperatures (573–973 K) were studied by EPR, UV–Visible–NIR DRS, temperature-programed reduction of sulfided samples (TPR-S), Z-contrast electron microscopy, and XRD. The catalysts were tested in the HDS of thiophene, dibenzothiophene, and 4,6-dimethyl-dibenzothiophene. Thiophene was chosen because this molecule can reach without impediments the active sites and consequently, the changes in the characteristics of the catalysts can be easily related to the observed changes in activity.

2. Experimental

2.1. Catalyst preparation

A Ru/TiO_2 catalyst with nominal Ru content of 2.1 ruthenium atoms per square nanometer of TiO_2, equivalent to 1.78 wt% Ru, was prepared using $RuCl_3{\cdot}xH_2O$ (Aldrich) as a precursor. TiO_2 Degussa P-25 with surface area of 52 m^2/g and pore volume of 0.9 cm^3/g was used as support.

To prepare the catalyst the precursor salt was dissolved in 2.5 times the volume of water needed to obtain incipient wetness (2.5×0.9 ml/g TiO_2). The solution was maintained under stirring for 12 h in N_2, the titania powder was added and the suspension was stirred for another 12 h. The catalyst was dried first in air flow at room temperature to eliminate the excess liquid and then in an oven at 383 K for 24 h. The solid was stored in a vacuum desiccator and was used without further drying for the experiments.

An alumina-supported catalyst Ru/Al_2O_3 with 2.1 ruthenium atoms per square nanometer of Al_2O_3 (equivalent to 7 wt% Ru) was also prepared with the procedure described above.

For thiophene, dibenzothiophene and 4,6-dimethyl-dibenzothiophene HDS, TPR-S, XRD, UV–Visible–NIR DRS, and EPR experiments the catalysts were sulfided for 2 h at different sulfidation temperatures (573, 673, 773, or 873 K) in a 15 ml/min H_2S(15 vol%)/N_2 stream.

2.2. Catalytic tests

2.2.1. Thiophene hydrodesulfurization

The catalytic tests were performed at atmospheric pressure in a continuous flow microreactor. The reaction products were analyzed by on-line gas chromatography (5890 Series II Hewlett Packard gas chromatograph). Prior to the catalytic tests the catalyst (100 mg) was sulfided *in situ* for 2 h with a 15 ml/min H_2S(15 vol%)/N_2 stream at 573, 673, 773, or 873 K. After sulfidation, a 20 ml/min stream of hydrogen saturated with thiophene at 275 K was contacted with the catalyst. Initially, the catalyst was maintained at a reaction temperature of 633 K until the conversion remained constant (~15 h), followed by measurements of thiophene conversion at different temperatures (from 593 to 493 K and back to 633 K).

2.2.2. Dibenzothiophene (DBT) and 4,6-dimethyl-dibenzothiophene (4,6-DMDBT) hydrodesulfurization

The catalytic tests were performed in a 350 ml Parr batch reactor. The reaction products were analyzed in a Varian CP-3800 chromatograph. Prior to the reaction test, the catalyst was sulfided at atmospheric pressure for 2 h with a 15 ml/min H_2S(15 vol%)/N_2 stream at 573 or 873 K, and was transferred to the batch reactor in argon atmosphere to avoid contact with air. The activity was measured at 593 K and 1300 psia for 9 h.

2.3. Characterizations

2.3.1. Temperature-programed reduction (TPR-S)

The experiments were carried out in a flow system equipped with a microreactor coupled to a Varian Cary 50 UV–Visible spectrometer to measure the evolution of H_2S at fixed wavelength and to a Gow-Mac Thermal Conductivity Detector (TCD) to calculate the amount of H_2 consumed during the sulfide reduction.

The TPR-S experiments were carried out with Ru/TiO_2 either freshly sulfided or used in the catalytic tests. In the first case the catalysts were sulfided *in situ*; in the second case, the catalysts used in the thiophene HDS experiment were immediately transferred to the TPR-S microreactor in argon atmosphere. For the reduction, the catalyst was heated in a 25 ml/min stream of H_2(70 vol%)/Ar at a constant rate of 10 K/min from room temperature to 1273 K. The reactor outlet stream was monitored by UV–Visible at 200 nm, and after removing H_2S in a trap, by TCD. As the traces obtained by TCD and UV–Visible showed similar behavior, only the H_2S evolution is reported here.

2.3.2. X-ray diffraction

The X-ray diffractograms of sulfided samples were registered with a Phillips 1050/25 diffractometer using Cu Kα radiation (λ = 1.5418 Å) and a goniometer speed of 1°(2θ) min^{-1}. The sulfided samples were transferred from the reactor to the diffractometer in argon atmosphere.

2.3.3. DRS-UV–Visible–NIR spectroscopy

The spectra of freshly sulfided catalysts were taken with a Cary 500 Varian spectrometer equipped with a diffuse reflectance sphere. The sulfided samples were transferred directly from the reactor to the sample holder in argon atmosphere.

2.3.4. Electron paramagnetic resonance (EPR)

The EPR experiments were carried out with freshly sulfided samples and with samples after thiophene HDS tests in a Bruker ELEXSYS-E500 spectrometer (X Band) at room temperature, 150, and 220 K. Only the spectra taken at 150 K are reported here. The sulfided sample was transferred to an EPR tube previously filled with argon; the tube was sealed and placed in the sample compartment.

2.3.5. Z-contrast electron microscopy

After 15 h under HDS reaction at 633 K, the sulfided catalysts were analyzed by Z-contrast in a Jeol JEM 2200 FS electron microscope. To avoid contact with air, the catalyst powder was transferred directly from the reactor filled with N_2 to a vial filled with *n*-heptane. One drop of the suspension catalyst–*n*-heptane was placed in a copper grid with carbon lacey, and, after evaporation at ambient conditions, the sample was introduced in the microscope.

3. Results and discussion

Ru/TiO_2 catalysts sulfided in $H_2S(15\%)/N_2$ at 573, 673, 773, and 873 K were tested in the thiophene HDS reaction at 493–593 K. At the beginning of each experiment, the catalyst was maintained at a reaction temperature of 633 K until the conversion remained constant (~15 h). An activation energy close to 69 kJ mol^{-1} was obtained for all catalysts. Hereafter, only the activity at 553 K is reported. For comparative purposes the HDS activity of an alumina-supported catalyst is also reported (Fig. 1 and Table 1) [19].

The Ru/TiO_2 catalyst sulfided at 573 K is remarkably active; its thiophene HDS activity is ~6 times bigger than that of Ru/Al_2O_3 sulfided at the same temperature. However, as the sulfidation temperature is raised, its HDS activity increases only slightly. In contrast, the alumina-supported catalyst displays low activity when sulfided at low temperature (573 K) but it is 10 times more active when sulfided at 973 K. In fact, at high sulfidation temperature the activity of Ru/Al_2O_3 is bigger than that of Ru/TiO_2. The fact that Ru/TiO_2 does not follow the same activity trend as Ru/Al_2O_3 with sulfidation temperature suggests that titania enhances the HDS activity only when the catalyst is sulfided at low temperature (573 K) but that it acts in detriment of the HDS activity when ruthenium is sulfided at high temperature.

The different response of Ru/TiO_2 and Ru/Al_2O_3 toward sulfidation temperature may arise from: (i) differences in the rate of RuS_2 sintering over titania and alumina, leading to significant differences in dispersion with the increase of sulfidation temperature, (ii) differences in the structure of the supported ruthenium sulfide phase, and/or (iii) differences in the electronic interaction between the supported phase and the titania or alumina supports. We will explore further these possibilities.

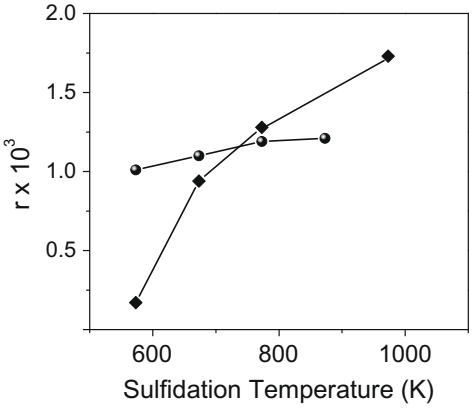

Fig. 1. HDS catalytic activity evaluated at 553 K. (●) Ru/TiO_2, (♦) Ru/Al_2O_3. Reaction rate in molecules of thiophene s^{-1} (Ru atom)$^{-1}$. Results of alumina-supported catalysts taken from [19].

Table 1
Catalytic activity at 553 K in the HDS of thiophene in alumina- and titania-supported ruthenium sulfide. The results of the alumina-supported catalyst are taken from [19].

Sulfidation temperature (K)	$r \times 10^3$ (molecule of thiophene s^{-1} (Ru atom)$^{-1}$)	
	Ru/TiO_2	Ru/Al_2O_3
973	–	1.73
873	1.21	–
773	1.19	1.28
673	1.10	0.94
573	1.01	0.17

The Z-contrast micrographs of Ru/TiO_2 sulfided at 873 K after 15 h of thiophene HDS show an average size of the RuS_2 particles of 2.6 nm. For the same Ru/Al_2O_3 catalyst it was reported earlier an average particle size of 2.2 nm when sulfided at 973 K [19]. Therefore, the small differences in particle size observed at high sulfidation temperature for the titania- and alumina-supported catalysts (2.6 and 2.2 nm, respectively) does not seem to explain the unexpectedly lower activity of Ru/TiO_2 sulfided at high temperature. Moreover, the FT-IR of adsorbed CO performed over Ru/Al_2O_3 catalysts suggested that the active sites available for HDS reaction are located at the edges and corners of the pyrite RuS_2 particles [19]. The percentage of such sites calculated using the RuS_2 model proposed in [20] is of 12% and 9% for particles of 2.2 nm (on alumina) and 2.6 nm (on titania), respectively. Therefore, it seems unlikely that the observed differences in catalytic activity between Ru/TiO_2 and Ru/Al_2O_3 are due to the differences in particle size.

Concerning the differences in ruthenium sulfide structure between Ru/TiO_2 and Ru/Al_2O_3, it was established before that the HDS activity on alumina-supported ruthenium sulfide strongly depends on the structure attained during the sulfidation step [19]. The changes in the structure of the supported ruthenium sulfide phase for Ru/TiO_2 sulfided at 573, 673, 773, and 873 K were analyzed here by X-ray diffraction (XRD) and temperature-programed reduction (TPR-S).

3.1. X-ray diffraction of the sulfided catalysts

For the XRD study a Ru/TiO_2 catalyst with 7 wt% Ru was prepared. This catalyst with higher Ru content was used only in the XRD characterization to be able to determine the changes in the ruthenium sulfide phase, assuming that the same behavior will be followed by the catalyst with lower Ru content (1.78 wt%) used in this work. The diffractograms of Ru/TiO_2-7 wt% sulfided at the different temperatures (Fig. 2) are dominated by peaks of titania (anatase and rutile). The increase in sulfidation temperature causes first the appearance then the growth of the main peaks of the RuS_2-pyrite phase (dotted vertical lines in Fig. 2). Moreover, subtracting the diffractogram of Ru/TiO_2-7 wt% sulfided at 573 K from those

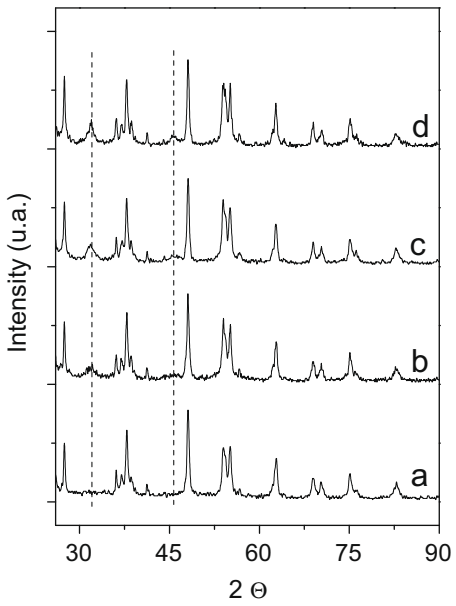

Fig. 2. X-ray diffractograms of Ru/TiO_2-7 wt% sulfided at (a) 573 K, (b) 673 K, (c) 773 K, and (d) 873 K. The dotted vertical lines correspond to the main diffraction peaks of the RuS_2-pyrite phase.

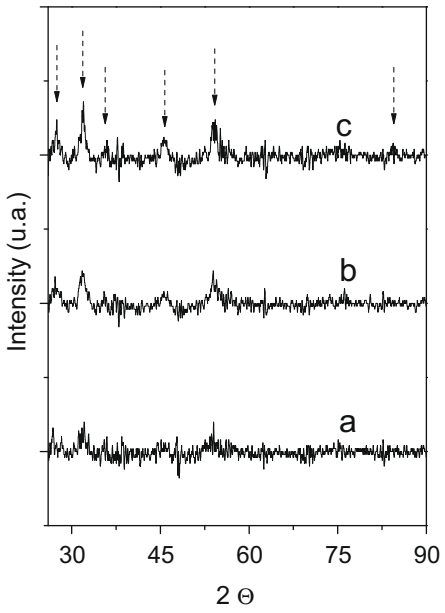

Fig. 3. Subtraction of X-ray diffractograms of sulfided Ru/TiO_2-7 wt%. (a) 673–573 K, (b) 773– 573, and (c) 873–573 K. The arrows point out the peaks associated to RuS_2-pyrite.

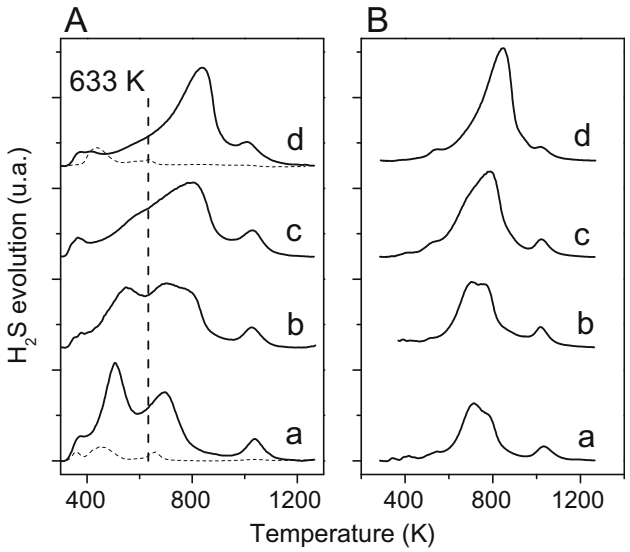

Fig. 4. TPR-S of Ru/TiO_2 freshly sulfided (Part A) and after thiophene HDS reaction (Part B). Sulfidation temperature (a) 573 K, (b) 673 K, (c) 773 K, and (d) 873 K. The reduction patterns of pure titania sulfided at (a) 573 and (d) 873 are shown in dotted lines. The temperature marked with a vertical line at 633 K is the one used in the thiophene HDS experiments to reach the steady-state operation of the catalyst.

obtained from catalysts sulfided at 673, 773, or 873 K it is clear that the increase in sulfidation temperature develops the peaks associated to RuS_2-pyrite (Fig. 3). The same behavior was observed for the alumina-supported catalysts. Since the subtraction diffractograms shown in Fig. 3 present only peaks of RuS_2-pyrite it can be concluded that no phase change occurs in titania (from anatase to rutile) during the sulfidation of the catalyst. Therefore, the different HDS activity responses with sulfidation temperature of Ru/TiO_2 compared to that of Ru/Al_2O_3 cannot be attributed to phase changes of the titania support.

3.2. Temperature-programed reduction (TPR-S)

The TPR-S experiments can detect if amorphous and/or pyrite ruthenium sulfides are formed at each sulfidation temperature.

Fig. 4A shows the reduction patterns of Ru/TiO_2 freshly sulfided at 573, 673, 773, and 873 K and those of pure titania freshly sulfided at 573 and 873 K. Comparison of the reduction patterns indicate that although TiO_2 is sulfided to some extent in accordance with the literature reports [17,21], the reduction observed for Ru/TiO_2 sulfided at the different temperatures arises mainly from the reduction of ruthenium sulfide species. The reduction that takes place at temperatures below ~410 K arises from the presence of excess sulfur [22–25]. The peak at ~515 K represents the reduction of RuS_2-amorphous and the asymmetric peak at temperatures higher than 633 K corresponds to the reduction of RuS_2-pyrite [19]. The small peak at ~1022 K most likely arises from the reduction of residual sulfur bonding the titania support to metallic Ru, formed during the reduction process. This reduction coincides with the beginning of the bulk reduction of titania evidenced by a large increase in the consumption of hydrogen, detected by the TCD (not shown).

From Fig. 4A, it is evident that the contribution of the RuS_2-amorphous to the total reduction patterns diminishes with the increase in sulfidation temperature due to crystallization into RuS_2-pyrite, the contribution of which grows, in agreement with the XRD results discussed above.

In the reduction patterns of the catalysts exposed to reaction for ~24 h (Fig. 4B) only the species that reduce at temperatures higher than 633 K are observed. This means that RuS_2-amorphous undergoes reduction during thiophene HDS while RuS_2-pyrite resists the reductive atmosphere prevailing in HDS reaction conditions. The two maxima or the asymmetry of the RuS_2-pyrite peak in all patterns in Fig. 4B are related to the two-step reduction, first the surface then the bulk, of RuS_2-pyrite particles [19,20,25]. This evidences that at a sulfidation temperature as low as 573 K, particles with pyrite structure in both surface and bulk are produced in Ru/TiO_2. In contrast, for Ru/Al_2O_3 it was concluded that the pyrite ruthenium sulfide particles produced at this low sulfidation temperature did not have pyrite structure on the surface [19]. This difference is relevant because the pyrite-type surfaces display better HDS activity.

The S/Ru ratios reported in Table 2 show a high sulfidation level in the freshly sulfided catalysts (S/Ru ~ 2.4). This is a consequence of the presence of elemental sulfur and the partial sulfidation of the titania surface [17,21], enhanced by the presence of the metal sulfide, as previously reported for W/TiO_2 catalysts [18]. For the catalyst sulfided at 573 K the S/Ru ratio decreases after thiophene HDS to 1.2 due to the reduction of RuS_2-amorphous. For the catalysts sulfided at higher temperatures the S/Ru ratio after HDS reaction increases with sulfidation temperature, in accordance with the bigger amount of RuS_2-pyrite in the catalyst, until it reaches a 2.2 value for the catalyst sulfided at 873 K. However, the considerable increase of the S/Ru ratio with sulfidation temperature is not reflected in a significant improvement of HDS activity, as it occurs for alumina-supported catalysts [19].

The XRD and TPR-S results indicate that the ruthenium sulfide phase has the same behavior when supported on alumina or tita-

Table 2
S/Ru ratio measured by TPR-S in catalysts freshly sulfided and after thiophene HDS reaction.

Sulfidation temperature (K)	Freshly sulfided	After thiophene HDS
873	2.3	2.2
773	2.3	2.0
673	2.4	1.7
573	2.3	1.2

nia: the increase in sulfidation temperature favors the transformation of RuS_2-amorphous into the more stable RuS_2-pyrite phase, leading to bigger S/Ru ratios under reaction conditions.

The differences in activity trend with sulfidation temperature displayed by Ru/TiO_2 and Ru/Al_2O_3 (Fig. 1 and Table 1), cannot be explained by differences in dispersion, structure or sulfidation behavior of the RuS_2 supported phase. To examine if these different activity trends are due to an electronic effect of the TiO_2 support on the Ru sulfided phase, UV–Visible–NIR DRS, and EPR experiments were conducted to analyze the electronic characteristics of the sulfided Ru/TiO_2.

3.3. Electronic properties of the sulfided catalysts

3.3.1. UV–Visible–NIR

The electronic spectra of pure titania unsulfided and freshly sulfided at 573 and 873 K are presented in Fig. 5. The unsulfided sample displays the typical UV–Visible–NIR DRS spectrum with no absorption in the NIR–Visible and absorption onset at 400 nm that corresponds to the charge transfer transition O2*p*–Ti3*d* in TiO_2 [26,27]. These characteristics define TiO_2 as a semiconductor with an energy gap of 3.66 eV. The absorption onset and the maximum in the spectra of titania freshly sulfided at 573 and 873 K have similar values, meaning that the electronic properties of titania do not change during the sulfidation process. The slight absorption in the entire interval and the smaller intensity in the charge transfer band in the spectrum of titania sulfided at 873 K suggest that titania has an incipient sulfidation at that temperature. The small signal between 360 and 620 nm (see insert in Fig. 5), attributed to forbidden transitions (consequently much less intense) of Ti^{3+} species in TiO_2 [17,28], indicates that sulfidation with $H_2S(15\%)/N_2$ at 873 K causes some reduction and therefore the appearance of Ti^{3+} in the support. The smaller intensity of the signal associated to Ti^{3+} compared to that of the charge transfer band does not reflect the relative amount of this species present in the catalyst because the signal comes from *d*–*d* transitions of a cation in an octahedral environment, which are much less intense than charge transfer signals [29].

As TiO_2, RuS_2 is a semiconductor with a band gap between 2.6 and 2.1 eV (477–590 nm) in supported particles [19,30]. In Fig. 6, the UV–Visible–NIR DRS spectra of Ru/TiO_2 freshly sulfided at 573 K (Fig. 6A) and at 873 K (Fig. 6B) present an absorption between 400 and 800 nm due to the RuS_2 phase since in that interval the absorption of TiO_2 sulfided at 573 K (Fig. 6A) and 873 K (Fig. 6B) is zero. For the sample sulfided at 873 K (Fig. 6B) the beginning of the absorption edge of RuS_2 is clearly observed at ~550 nm, previous to the absorption edge of the much more intense charge transfer band of titania.

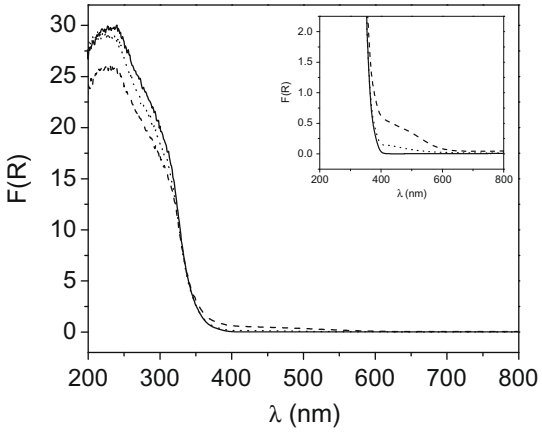

Fig. 5. UV–Visible–NIR DRS spectra of TiO_2 (– – –) sulfided at 873 K, (···) sulfided at 573 K, and (—) unsulfided.

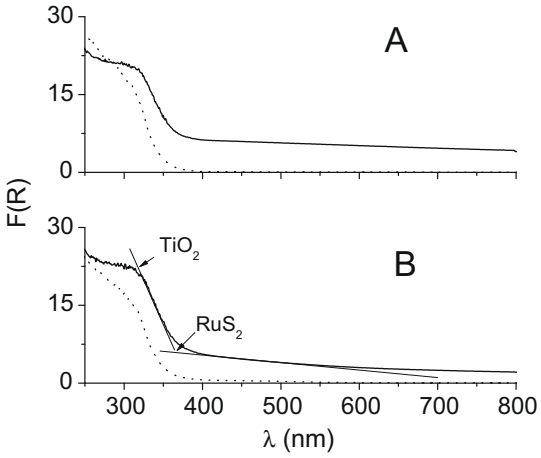

Fig. 6. UV–Visible–NIR DRS spectra of TiO_2 (dotted lines) and Ru/TiO_2 (solid lines) sulfided at 573 K (A) and 873 K (B).

The absorption at wavelengths above ~550 nm reveals the presence of defects in the sulfided particles in both samples. It is known that the structural defects give rise to localized electronic states within the band gap and therefore, to electronic transitions from the valence band toward the electronic states associated to defects at energies below that of the band gap [31]. The higher absorbance of Ru/TiO_2 sulfided at 573 K compared to the sample sulfided at 873 K (i.e., $F(R) = 4.2$ and 2.1 at $\lambda = 800$ nm, respectively) corresponds well with the highly defective RuS_2-amorphous structure present in the catalyst sulfided at 573 K. The continuous increase in the absorption from 800 to ~550 nm in the spectrum of Ru/TiO_2 sulfided at 573 K also reveals, in agreement with the TPR-S results, the presence of an amorphous material (RuS_2-amorphous) in the catalyst [19,31]. The localized electronic states associated to sulfur vacancies at the surface of ruthenium sulfide particles with pyrite structure in both bulk and surface, which are also structural defects, are responsible for the absorption above 477–590 nm (2.1–2.6 eV) in Ru/TiO_2 sulfided at 873 K.

It is observed in Fig. 6 that the charge transfer band of titania shifts toward higher wavelengths in Ru/TiO_2 sulfided at both temperatures, evidencing that the presence of ruthenium sulfide on the surface of titania modifies the electronic properties of the support. The absorption edge shift, from 3.66 eV in pure titania to 3.40 eV in sulfided Ru/TiO_2, suggests that the beginning of the conduction band of RuS_2 is located in the band gap of titania, just below the lower limit of the conduction band, as illustrated in Scheme 1. This result is important since it shows that in the sulfided catalysts the conduction band of titania and that of ruthenium sulfide are connected and form one single band. This combined effect of semiconductors is observed in several catalytic systems [30,32,33].

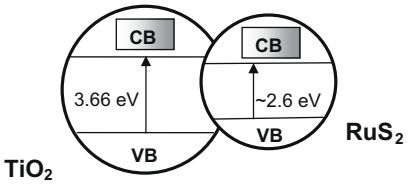

Scheme 1. Band gap transitions in titania and ruthenium sulfide.

3.3.2. Electron paramagnetic resonance

To analyze the role of each species present in the sulfided catalysts, that is, TiO_2, RuS_2-amorphous, RuS_2-pyrite and $TiO_{2-x}(Ti^{3+})$, a detailed EPR study was conducted with freshly sulfided and after thiophene HDS catalysts.

Due to its electronic structure, full valence band and empty conduction band with no unpaired electrons, TiO_2 does not present species active in EPR. However, reductive treatments cause the appearance of strong EPR signals associated to Ti^{3+} species and to positive holes in the conduction band [32,34,35]. It was also reported that only 10% of the promoted electrons are trapped in localized states in Ti^{3+} and are active in EPR. The rest of the electrons (90%) are in the conduction band and are silent to EPR [34,36]. Table 3 summarizes the values of g reported for species of Ti and Ru active in EPR.

3.3.2.1. Catalysts sulfided at 873 K. Fig. 7 presents the EPR spectra at 150 K of TiO_2 freshly sulfided, Ru/TiO_2 freshly sulfided, and after thiophene HDS. The EPR spectrum of titania freshly sulfided at 873 K has a single isotropic signal with $g = 1.952$ (Fig. 7a). The width from peak to peak is 110 Gauss and that of the entire signal is about 600 Gauss. As shown in Table 3 the signal at $g = 1.952$ can be assigned to electrons trapped in Ti^{3+}, in agreement with the UV–Visible–NIR results discussed above, that revealed the presence of Ti^{3+} in the sulfided sample. The absence of signals associated to holes trapped in oxygen ($g \sim 2.003$) is probably related to an inefficiency of the lattice due to a high concentration of electrons in excited states, as has been explained for titania reduced with vacuum and heat [34]. The formation of Ti^{3+} in TiO_2 during sulfidation at 873 K can be explained through a reduction process in which oxygen is removed from the solid as molecular oxygen by the effect of temperature and then carried away by the $H_2S(15\%)/N_2$ sulfiding stream.

The EPR spectrum of Ru/TiO_2 freshly sulfided at 873 (Fig. 7b) consists of (a) an isotropic signal at $g = 1.952$, peak to peak width of 110 Gauss, assigned to electrons trapped in Ti^{3+}, (b) traces of a signal at $g = 2.008$, which can be assigned to holes in the valence band as shown in Table 3, and (c) a wide signal present at $2.274 > g > 2.047$. This last signal does not correspond to species of titanium since they have g values lower than 2.0023 [37]. It possibly comes from electrons associated to ruthenium. In fact, the g values of the Ru species active in EPR reported in Table 3 vary from 2.68 to 2.06. The EPR signals of electrons associated to ruthenium

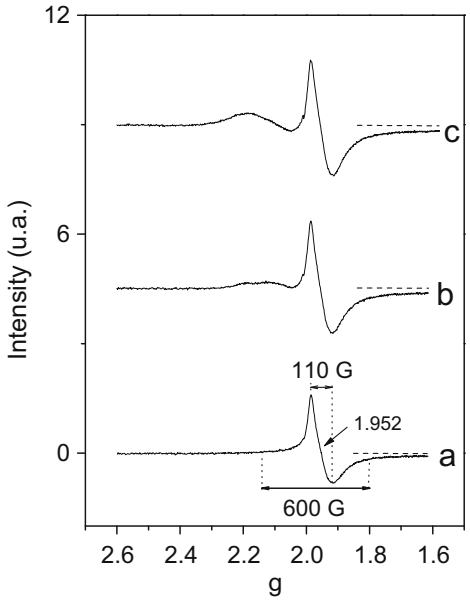

Fig. 7. EPR spectra of samples sulfided at 873 K. (a) TiO_2 freshly sulfided, (b) Ru/TiO_2 freshly sulfided, and (c) Ru/TiO_2 after thiophene HDS. EPR experiments made at 150 K.

Table 3
Species active in EPR.

Species	g_1 $g_\parallel$	g_2 $g_\perp$	g_3	References (and references therein)
Ti^{3+} in the surface	1.957	1.990	1.990	[35]
Ti^{3+} in the bulk	1.961	1.992	1.992	
Ti^{3+} in the surface	1.954	1.972	–	[54]
Ti^{3+} in the bulk	–	1.990	–	
Ti^{3+} in the surface	1.954	1.978	–	[55]
Ti^{3+} in the bulk	–	1.988	–	
Ti^{3+} in the surface	1.958	1.988	–	[56]
Ti^{3+} in the bulk	1.962	1.991	–	
Ti^{3+}(I)	1.949	1.964	–	[34,57]
Ti^{3+}(II)	1.960	1.990	–	
Ti^{3+}	–	1.991	–	[32]
	1.931	1.987	1.996	[53]
		1.998		[58]
Ti^{3+} in compounds with octahedral coordination	1.95			[59]
$Ti^{4+}O^{1-}$–$Ti^{4+}OH^{1-}$	2.004	2.014	2.018	[35]
	2.002	2.011	2.018	[56]
$Ti^{4+}O^{2-}$–$Ti^{4+}O^{1-}$	2.004	2.018	2.030	[35]
	2.003	2.014	2.026	[56]
	2.007	2.014	2.025	[54]
Holes trapped in oxygen in the surface of TiO_2	–	2.002	–	[55]
Holes trapped in O^{1-} anions	2.0046	2.012	–	[57,34]
$Ti^{4+}O^{2-}$	2.003–2.007	2.029	–	[32]
Free spin	–	2.0023	–	
Ru^{1+}	1.995	2.177	–	[60,61]
Ru^{3+}	1.72–1.79	2.06–2.28	–	[38]
Ru^{3+}	1.72–2.24	2.08–2.68	1.71–1.95	[62]

are wider (e.g. ~900 Gauss from peak to peak in Ru^{3+} [38]) than those of species associated to titania (110 Gauss, Fig. 7a). Consequently, the spectrum of Ti^{3+} is located within the spectrum of the species associated to ruthenium. This explains why only the beginning of the signal associated to ruthenium is observed and the different level of the base line at ~1.6 g, emphasized by the dotted line in Fig. 7b. The EPR spectrum of Ru/TiO_2 after thiophene HDS (Fig. 7c) retains the features of the freshly sulfided catalyst, in agreement with the TPR-S results that showed that the catalyst sulfided at 873 K does not change significantly during reaction.

3.3.2.2. Catalysts sulfided at 573 K. Fig. 8 presents the EPR spectra at 150 K of TiO_2 freshly sulfided, Ru/TiO_2 freshly sulfided, and after thiophene HDS. The spectrum of TiO_2 freshly sulfided at 573 K shows only traces of signals associated to electrons trapped in Ti^{3+} and to holes trapped in oxygen (Fig. 8a), in agreement with the UV–Visible–NIR results that showed that the electronic characteristics of titania do not change during sulfidation at this temperature (Fig. 5). These results indicate that titania is not reduced during sulfidation at 573 K.

The spectrum of Ru/TiO_2 freshly sulfided at 573 K (Fig. 8b) is deeply different from that of titania freshly sulfided at 573 K (Fig. 8a) and to that of Ru/TiO_2 freshly sulfided at 873 K (Fig. 7b). The spectrum is dominated by a wide isotropic signal at $g = 2.047$ with a width of 966 Gauss. Due to its g value the signal is not associated to titanium [36]; neither to holes in spite of its proximity to the values reported in Table 3, since the peak to peak width associated to holes is around 12 Gauss (see for example spectra in [34,39]), very different from the width of the spectra shown in Fig. 8b. Only traces of signals arising from Ti^{3+} and holes are present at $g = 2.007$, 1.983, and 1.926. Therefore, the wide signal at $g = 2.047$ that dominates the EPR spectrum shown in Fig. 8b can be associated to paramagnetic ruthenium species.

The wide signal at $g = 2.047$ is not due to paramagnetic Ru^{3+} in residual unsulfided ruthenium chloride because in the EPR spectrum of unsulfided Ru/TiO_2 (not shown) no paramagnetic species were detected and only traces of signals at $g = 2.2$ and 2.6 were observed. This result indicates, in agreement with the previous literature reports [40], that the oxidation state in the commercial ruthenium chloride used here is Ru^{4+} (EPR silent [37]) or a mixture of Ru^{3+}/Ru^{4+} that do not produce an EPR signal [41]. Therefore, the wide signal at $g = 2.047$ is assigned to the presence of paramagnetic ruthenium species in ruthenium sulfide.

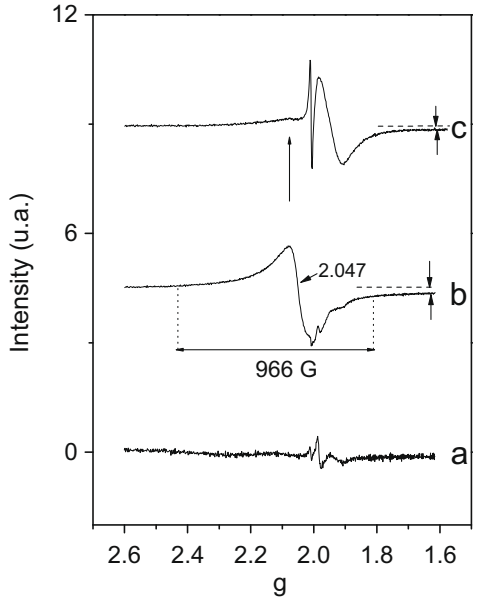

Fig. 8. EPR spectra of samples sulfided at 573 K. (a) TiO_2 freshly sulfided, (b) Ru/TiO_2 freshly sulfided, and (c) Ru/TiO_2 after thiophene HDS. EPR experiments made at 150 K.

Since ruthenium sulfide is diamagnetic (d^6, low spin), the EPR signal in Ru/TiO_2 freshly sulfided at 573 K can be explained invoking the presence of localized electronic states associated to structural defects. The presence of structural defects in this catalyst was evidenced also by the absorption of energy between 800 and 550 nm in the UV–Visible–NIR spectrum (Fig. 6A). This energy absorption gives rise to transitions from the valence band toward localized states generating the appearance of paramagnetic species which are detected in the EPR spectrum. Paramagnetic signals associated to defects can be detected not only in amorphous ruthenium sulfide as shown here but also in single crystals of RuS_2 [42,43]. This result indicates, in line with the TPR-S results, that with sulfidation at 573 K a highly defective ruthenium sulfide (RuS_2-amorphous) is produced on the catalytic surface. Furthermore, unlike the spectra of the samples sulfided at 873 K, the spectrum of the catalyst sulfided at 573 K is observed not only at 150 K but also at room temperature (spectrum not shown), indicating the different natures of the sulfided phase in each case, and suggesting that the dissipation of vibrational, rotational, and translational energies when returning to the basal state [39] is less efficient in the defective structure than in crystalline RuS_2-pyrite.

The characteristics of the spectrum of Ru/TiO_2 freshly sulfided at 573 K (Fig. 8b) arise from electronic states associated to structural defects in amorphous ruthenium sulfide. The EPR spectrum of the catalyst after thiophene HDS (Fig. 8c) is different from that of Ru/TiO_2 freshly sulfided. It is dominated by two signals, one intense sharp signal at $g = 2.008$ with peak to peak width of 11 Gauss and another at $g = 1.947$ with peak to peak width of 131 Gauss. The two signals are associated to TiO_2: the first one to holes in the valence band and the second one to electrons trapped in Ti^{3+} (see Table 3). This result indicates that titania suffers reduction during the HDS reaction, in accordance to literature reports that showed that in the case of pure TiO_2 it is relatively easy to reduce Ti^{4+} to Ti^{3+} in a hydrogen atmosphere at the reaction temperatures used here [44–46]. It has also been reported that sulfided titania is reduced when treated in hydrogen at high temperature [21].

After HDS reaction, the signal associated to RuS_2-amorphous almost disappears as pointed out by the arrow in Fig. 8, corroborating that during the HDS reaction RuS_2-amorphous is reduced and consequently, the defective structures are no longer present in the catalytic surface. Accordingly, the TPR-S results after reaction indicate that the S/Ru ratio decreases to 1.2 during HDS (Table 2). Since the TPR-S detects only RuS_2-pyrite, it is very likely that small domains of metallic ruthenium coexist on the surface with RuS_2-pyrite. Other studies have reported the presence of metallic Ru domains after HDS reaction for Ru/zeolite sulfided catalysts [47]. Therefore, the high intensity of the sharp signal at $g = 2.008$ in Fig. 8c, which indicates a high population of holes in the valence band of titania, might be a consequence of the presence of the small domains of metallic ruthenium which operate as efficient electron scavengers [28,48]. This signal is not present in Ru/TiO_2 sulfided at 873 K after HDS (Fig. 7c), where metallic ruthenium is absent.

3.3.2.3. EPR of alumina-supported ruthenium sulfide. To corroborate the EPR assignments for ruthenium sulfide in Ru/TiO_2, additional experiments were made with Ru/Al_2O_3 (Fig. 9) because in the latter case Ru sulfide is supported on an insulator (with no EPR active species), which means that the RuS_2 particles are isolated and do not interact electronically with the support. The EPR spectra of Ru/Al_2O_3 freshly sulfided at the lower temperature (573 K, Fig. 9a) show a strong signal of paramagnetic ruthenium species

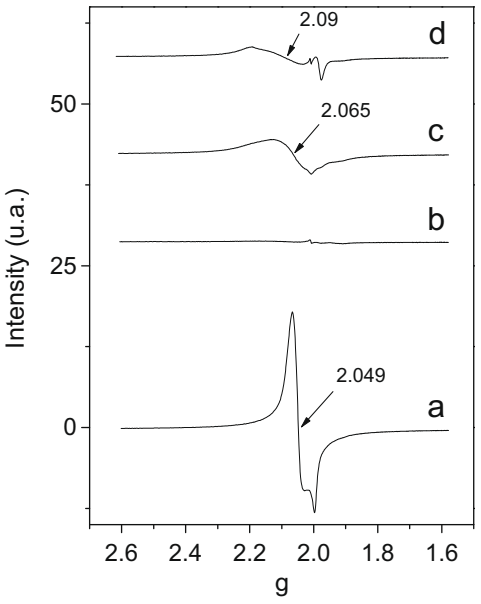

Fig. 9. EPR spectra of Ru/Al_2O_3 freshly sulfided at 573 K and after thiophene HDS (a) and (b). Freshly sulfided at 873 K and after thiophene HDS (c) and (d).

at $g = 2.049$, assigned to structural defects in RuS_2, that completely disappears after thiophene HDS (Fig. 9b). In contrast, when Ru/Al_2O_3 is sulfided at 873 K, the signal of paramagnetic ruthenium is much less intense and slightly shifted to $g = 2.065$ (Fig. 9c), indicating that fewer defects are present in RuS_2. This is no surprising since the crystallinity of ruthenium sulfide increases with the sulfidation temperature. The shape of the spectrum suggests that it is formed by two signals, probably arising from two different structural environments; only one of them disappears after thiophene HDS (Fig. 9d). So, it appears that the signal obtained with sulfidation at 873 K corresponds to surface structural defects, that is, to surface cations in RuS_2-pyrite with incomplete coordination. The small signal observed at $g = 2.007$ in the spectra (Fig. 9a) and (Fig. 9d) has been reported as due to sulfur radicals trapped in the smallest pores of alumina [49].

The above-mentioned results show that the EPR signals associated to ruthenium sulfide in Ru/TiO_2 are also present in Ru/Al_2O_3, indicating that ruthenium sulfide has the same electronic characteristics when deposited on titania or alumina. However, when supported on titania additional effects arising from electronic transfers between the Ru species and the TiO_2 support affect the performance of the catalyst during the HDS reaction. In what follows we will explain why the performance of Ru/TiO_2 is different from Ru/Al_2O_3 when the sulfidation temperature is varied.

3.4. Catalytic activity in Ru/TiO_2 HDS catalysts

It has been well established that the HDS activity of Ru/Al_2O_3 increases significantly with the sulfidation temperature (Fig. 1) because a larger amount of RuS_2-pyrite phase both on surface and in bulk is formed at high sulfidation temperature [19]. It was expected that the Ru/TiO_2 catalyst would behave similarly, displaying even higher activity than Ru/Al_2O_3 because it has been reported that titania is able to promote the HDS activity of transition metal sulfides [17,18]. In fact, Fig. 1 shows that at low sulfidation temperature the activity of Ru/TiO_2 is high (six times that of Ru/Al_2O_3). However, at this sulfidation temperature in both catalysts the RuS_2 phase is mostly as RuS_2-amorphous that is reduced under reaction conditions. So, the high activity of Ru/TiO_2 must be explained by other than the presence of RuS_2-pyrite. Unlike Ru/Al_2O_3, when the sulfidation temperature is raised, only a slight increase in the HDS activity is observed for Ru/TiO_2 in spite of the increase in the surface concentration of well-crystallized RuS_2-pyrite phase, which should enhance the HDS activity. It appears then that TiO_2 does not promote the activity of RuS_2-pyrite but, on the contrary, it diminishes its catalytic activity.

To explain the lower HDS activity of Ru/TiO_2 compared to Ru/Al_2O_3 at high sulfidation temperature it is necessary to rationalize the effect of the electronic transfer from titania toward RuS_2-pyrite, evidenced by the UV–Visible–NIR and EPR experiments. On the one hand, the localized electronic states of Ti^{3+} observed in the EPR spectrum of RuS_2/TiO_2 sulfided at 873 K (Fig. 7c) are an indicator of the presence of EPR silent electrons in the conduction band of TiO_2 [34,36]. On the other hand, the UV–Visible–NIR results (Fig. 6) show that the conduction bands of titania and RuS_2-pyrite are connected (see Scheme 1). This means that the EPR silent electrons are delocalized in the conduction bands of both titania and RuS_2-pyrite, formed by the antibonding $Ru4de_g^*$—$S3p\sigma^*$ hybrid states [8,50]. This has a negative effect on the HDS activity since it impinges e_g character to the HOMO, which already had an optimum configuration of 6 electrons in t_{2g} orbitals [5–9]. The non-t_{2g} character of the occupied electronic states in PdS and PtS has been used to explain the lower HDS activity of these sulfides compared to RuS_2 [8]. The additional electronic density supplied to RuS_2-pyrite by titania is received in the conduction band, which is oriented in the direction of the Ru–S bond and of the sulfur vacancies at the surface of RuS_2-pyrite crystallites, playing an inhibiting role for the adsorption of sulfur-containing organic molecules such as thiophene. Results from theoretical calculations showed that when the interaction between the metal *d*orbitals and the sulfur 3*p* lone pair of the thiophene molecule is strong, the activity is high [51]. The two effects described above act in detriment of the HDS activity of RuS_2-pyrite supported on titania and explain why its activity in thiophene HDS is lower than that of RuS_2-pyrite supported on Al_2O_3. Areal reaction rates (thiophene molecules s^{-1} nm^{-2} of RuS_2 particle surface) at high sulfidation temperature, where the Ru phase is well defined and consists only of RuS_2-pyrite, for Ru/TiO_2 and Ru/Al_2O_3 are 0.019 and 0.025, respectively, confirming the lower activity of the Ru/TiO_2 system.

The findings of this work provide experimental evidence to the theoretical correlations between the electronic structure of transition metal sulfides and HDS activity [5–9]. Our results show that transferring electronic density to a transition metal sulfide such as RuS_2, in which Ru already has full HOMO of nature t_{2g}, diminishes its HDS activity. They also contribute to better understand that the role of the promoter in HDS catalysts is to provide electronic density to transition metals with electron deficiencies in the t_{2g} orbitals.

At low sulfidation temperature (573 K) Ru/TiO_2 is ~6 times more active in HDS than Ru/Al_2O_3. At this sulfidation temperature the catalytic system is different from Ru/TiO_2 sulfided at 873 K because after reaction besides RuS_2-pyrite and TiO_{2-x} (Ti^{3+}), small domains of metallic ruthenium (product of RuS_2-amorphous reduction) are present on the surface. In the case of Ru/Al_2O_3 sulfided at 573 K small domains of metallic ruthenium and RuS_2-pyrite with sulfur depleted surface are present after reaction [19].

An explanation for the better performance of Ru/TiO_2 sulfided at 573 K arises from the interaction between the titania support and the metallic ruthenium particles produced during the reduction of RuS_2-amorphous. Previous studies made with ruthenium sulfide containing small domains of metallic ruthenium, showed that both dissociate hydrogen and that the bond strength of Ru–H is weaker than that of RuS–H. The results showed that the Ru–H species played an important role in hydrogen activation [52, and references therein]. In the case of Ru/TiO_2, it is likely that the electron density transferred from titania to the metallic ruthenium do-

Table 4
Catalytic activity in the HDS of DBT and 4,6-DMDBT in alumina- and titania-supported ruthenium sulfide ($T_{reaction}$ = 593 K, P = 1300 psig).

	$r \times 10^5$ (molecule DBT (4,6-DMDBT) s^{-1} (Ru atom)$^{-1}$)	
	$T_{sulfidation}$ = 573 K	$T_{sulfidation}$ = 873 K
Ru/Al_2O_3		
DBT	13	83
4,6-DMDBT	8	27
Ru/TiO_2		
DBT	28	56
4,6-DMDBT	17	21

mains, evidenced by EPR in Fig. 8c, weakens the Ru–H bonds, augmenting the capacity to supply hydrogen to the HDS reaction, that takes place on the surface of the remaining particles of RuS_2-pyrite. This effect may substantially increase the HDS activity of Ru/TiO_2 sulfided at 573 K. In agreement with this proposal, small Pd particles supported on titania have been found to activate hydrogen due to Ti^{3+}–metal interaction [53]. As the sulfidation temperature is raised, the amount of metallic ruthenium on the catalytic surface decreases because its precursor, the RuS_2-amorphous phase, is progressively transformed into the more stable RuS_2-pyrite phase. This then eliminates the beneficial effect of the interaction titania–Ru^0 to activate hydrogen.

It appears then that the HDS activity of Ru/TiO_2 catalysts at the different sulfidation temperatures is the result of several opposing effects:

(i) At low sulfidation temperature, where most of the RuS_2 is amorphous and reduces to Ru^0 during HDS, the electronic transfer from TiO_2 to the Ru metallic domains enhances the activation of hydrogen increasing the supply of hydrogen for the HDS reaction that takes place on the surface of the remaining RuS_2 particles with pyrite structure.
(ii) As the sulfidation temperature is raised, the concentration of metallic domains of Ru decreases in favor of the formation of RuS_2-pyrite, which in itself has high HDS activity. However, when supported on TiO_2 receives electronic transfers that alter the configuration of 6 electrons at the HOMO, which has been reported as the optimum for HDS activity [5–9]. Moreover, it is very likely that the additional electronic density in the direction of the Ru–S bond inhibits the adsorption of the sulfur-containing organic molecule on the sulfur vacancies during HDS.

Catalytic HDS tests performed in batch reactor using more refractory sulfur-containing molecules such as dibenzothiophene and 4,6-dimethyl-dibenzothiophene confirmed the activity trends observed for thiophene between HDS activity and catalyst sulfidation temperature (see Table 4).

4. Conclusion

The dispersion and structure of the ruthenium sulfided phase formed at the different sulfidation temperatures are essentially the same when supported on alumina or titania. However, when supported on titania additional effects arising from electronic transfers between the Ru species and the TiO_2 support affect the performance of the catalyst during the HDS reaction.

At low sulfidation temperature (573 K) a mixture of RuS_2-amorphous and RuS_2-pyrite is produced on the catalyst surface. The increase in sulfidation temperature favors the formation of RuS_2-pyrite in detriment of RuS_2-amorphous. The former is a stable phase that remains unaltered under HDS reaction conditions while the latter is unstable and undergoes reduction, producing Ru^0.

The high HDS activity of Ru/TiO_2 sulfided at 573 K is explained through the interaction between metallic Ru and titania.

The unexpectedly low HDS activity of Ru/TiO_2 sulfided at 873 K is explained because in this case the electronic density supplied by titania alters the already optimum electronic configuration of 6 electrons at the HOMO of ruthenium sulfide (full t_{2g} orbitals).

The same activity-sulfidation temperature trend is observed for the HDS of thiophene, dibenzothiophene, and 4,6-dimethyl-dibenzothiophene.

The findings of this work provide experimental evidence to the reported theoretical correlations between electronic structure and HDS activity.

Acknowledgments

We are indebted to DGAPA–UNAM program (IN-102709) for financial support. We acknowledge Alejandro Solano for the EPR experiments and helpful discussions, Cecilia Salcedo for the XRD experiments, Carlos Ángeles Chávez for his help in the Z-contrast characterization, Iván Puente for TEM work, and Rogelio Cuevas for his help in the reaction experiments. P. Castillo-Villalón acknowledges Dr. Rafael Moreno for helpful discussions.

References

[1] T.A. Pecoraro, R.R. Chianelli, J. Catal. 67 (1981) 430.
[2] N. Hermann, M. Brorson, H. Topsøe, Catal. Lett. 65 (2000) 169.
[3] A.P. Raje, S.-J. Liaw, R. Srinivasan, B.H. Davis, Appl. Catal. A 150 (1997) 297.
[4] M. Lacroix, H. Marrakchi, C. Calais, M. Breysse, C. Forquy, Stud. Surf. Sci. Catal. 59 (1991) 227.
[5] S. Harris, R.R. Chianelli, J. Catal. 86 (1984) 400.
[6] R.R. Chianelli, Oil Gas Sci. Technol.: Rev. IFP 61 (2006) 503.
[7] R.R. Chianelli, M. Daage, M.J. Ledoux, Adv. Catal. 40 (1994) 177.
[8] P. Raybaud, J. Hafner, G. Kresse, H. Toulhoat, J. Phys.: Condens. Matter 9 (1997) 11107.
[9] P. Raybaud, G. Kresse, J. Hafner, H. Toulhoat, J. Phys.: Condens. Matter 9 (1997) 11085.
[10] S. Harris, R.R. Chianelli, J. Catal. 98 (1986) 17.
[11] R.R. Chianelli, G. Berhault, P. Raybaud, S. Kasztelan, J. Hafner, H. Toulhoat, Appl. Catal. A 227 (2002) 83.
[12] J. Ramírez, S. Fuentes, G. Díaz, M. Vrinat, M. Breysse, M. Lacroix, Appl. Catal. 52 (1989) 211.
[13] E. Olguín, M. Vrinat, L. Cedeño, J. Ramírez, M. Borque, A. López-Agudo, Appl. Catal. A 165 (1997) 1.
[14] J. Ramírez, A. Gutiérrez-Alejandre, J. Catal. 170 (1997) 108.
[15] J. Ramírez, A. Gutiérrez-Alejandre, Catal. Today 43 (1998) 123.
[16] M. Borque, A. López-Agudo, E. Olguín, M. Vrinat, L. Cedeño, J. Ramírez, Appl. Catal. A 180 (1999) 51.
[17] J. Ramírez, L. Cedeño, G. Busca, J. Catal. 184 (1999) 59.
[18] J. Ramírez, G. Macías, L. Cedeño, A. Gutiérrez-Alejandre, R. Cuevas, P. Castillo-Villalón, Catal. Today 98 (2004) 19.
[19] P. Castillo-Villalón, J. Ramírez, F. Maugé, J. Catal. 260 (2008) 65.
[20] C. Geantet, C. Calais, M. Lacroix, C.R. Acad. Sci. Paris 315 (1992) 439.
[21] D. Wang, W. Qian, A. Ishihara, T. Kabe, J. Catal. 203 (2001) 322.
[22] J.A. De Los Reyes, M. Vrinat, C. Geantet, M. Breysse, J.G. Grimblot, J. Catal. 142 (1993) 455.
[23] J.A. De Los Reyes, M. Vrinat, C. Geantet, M. Breysse, Catal. Today 10 (1991) 645.
[24] G. Berhault, M. Lacroix, M. Breysse, F. Maugé, J.C. Lavalley, L. Qu, J. Catal. 170 (1997) 37.
[25] F. Lebruyère, M. Lacroix, D. Schweich, M. Breysse, J. Catal. 167 (1997) 464.
[26] J. Ramírez, L. Ruiz-Ramírez, L. Cedeño, V. Harle, M. Vrinat, M. Breysse, Appl. Catal. A 93 (1993) 163.
[27] H. Bevan, S.V. Dawes, R.A. Ford, Spectrochim. Acta 13 (1958) 43.
[28] D.W. Bahnemann, M. Hilgendorff, R. Memming, J. Phys. Chem. B 101 (1997) 4265.
[29] J. Huheey, E. Keiter, R. Keiter, Inorganic Chemistry – Principles of Structure and Reactivity, Harper Collins College Publishers, New York, 1993. p. 440.
[30] K. Hara, K. Sayama, H. Arakawa, Appl. Catal. A 189 (1999) 127.
[31] W. Hayes, A.M. Stoneham, Defects and Defects Processes in Nonmetallic Solids, Dover Publications, Mineola, NY, 2004. p. 386.
[32] L. Wu, J.C. Yu, X. Fu, J. Mol. Catal. A: Chem. 244 (2006) 25.
[33] F. Bosc, D. Edwards, N. Keller, V. Keller, A. Ayral, Thin Solid Films 495 (2006) 272.
[34] T. Berger, M. Sterrer, O. Diwald, E. Knözinger, D. Panayotov, T.L. Thompson, J.T. Yates Jr., J. Phys. Chem. B 109 (2005) 6061.
[35] Y. Nakaoka, Y. Nosaka, J. Photochem. Photobiol. A 110 (1997) 299.
[36] A. Yamakata, T.-a. Ishibashi, H. Onishi, Chem. Phys. Lett. 333 (2001) 271.

[37] R.S. Drago, Physical Methods for Chemists, Saunders College Publishing, 1992. p. 566, 581.
[38] P. Castillo-Villalón, J. Ramírez, M.J. Peltre, C. Louis, P. Massiani, Phys. Chem. Chem. Phys. 6 (2004) 3739.
[39] M. Che, E. Giamello, Catalyst Characterization. Physical Techniques for Solid Materials, Plenum Press, New York, 1994. p. 133.
[40] E.A. Seddon, K.R. Seddon, The Chemistry of Ruthenium, Elsevier, Amsterdam, Oxford, New York, Tokio, 1984. p. 159.
[41] M. Goldwasser, J.F. Dutel, C. Naccache, Zeolites 9 (1989) 54.
[42] J.-T. Yu, S.-S. Lin, Y.S. Huang, J. Appl. Phys. 68 (1990) 1796.
[43] J.-T. Yu, S.-S. Lin, Y.S. Huang, J. Appl. Phys. 65 (1989) 4230.
[44] W. Zhaobin, X. Qin, G. Xiexian, E. Sham, P. Grange, B. Delmon, Appl. Catal. 63 (1990) 305.
[45] W. Zhaobin, X. Qin, G. Xiexian, P. Grange, B. Delmon, Appl. Catal. 75 (1991) 179.
[46] P. Panagiotopoulou, A. Christodoulakis, D.I. Kondarides, S. Boghosian, J. Catal. 240 (2006) 114.
[47] B. Moraweck, G. Bergeret, M. Cattenot, V. Kougionas, C. Geantet, J.L. Portefaix, J.L. Zotin, M. Breysse, J. Catal. 165 (1997) 45.
[48] A.L. Linsebigler, G. Lu, J.T. Yates Jr., Chem. Rev. 95 (1995) 735.
[49] S. Kowalak, A. Jankowska, S. Zeidler, A.B. Wieckowski, J. Solid State Chem. 180 (2007) 1119.
[50] S.-S. Lin, J.-K. Huang, Y.-S. Huang, Mod. Phys. Lett. B 7 (1993) 271.
[51] T.S. Smit, K.H. Johnson, Catal. Lett. 28 (1994) 361.
[52] M. Breysse, E. Furimsky, S. Kasztelan, M. Lacroix, G. Perot, Catal. Rev. 44 (2002) 651.
[53] J. Panpranot, K. Kontapakdee, P. Praserthdam, J. Phys. Chem. B 110 (2006) 8019.
[54] S.W. Ahn, L. Kevan, J. Chem. Soc., Faraday Trans. 94 (1998) 3147.
[55] Z. Luan, L. Kevan, Micropor. Mesopor. Mater. 44–45 (2001) 337.
[56] S.-C. Ke, T.-C. Wang, M.-S. Wong, N.O. Gopal, J. Phys. Chem. B 110 (2006) 11628.
[57] T. Berger, M. Sterrer, S. Stankic, J. Bernardi, O. Diwald, E. Knözinger, Mater. Sci. Eng. C 25 (2005) 664.
[58] E. Muñoz, J.L. Boldú, E. Andrade, O. Novaro, X. Bokhimi, T. López, R. Gómez, J. Am. Ceram. Soc. 84 (2001) 392.
[59] H.A.O. Hill, P. Day, Physical Methods in Advanced Inorganic Chemistry, Interscience Publishers, London, New York, Sydney, 1968. p. 316.
[60] G.I. Pilipenko, A.A. Sabirzyanov, V.G. Stepanov, D.V. Oparin, V.V. Izotov, F.F. Gavrilov, J. Phys.: Condens. Matter 4 (1992) 4047.
[61] G.I. Pilipenko, A.A. Sabirzyanov, D.V. Oparin, V.G. Stepanov, F.F. Gavrilov, J. Phys.: Condens. Matter 4 (1992) 4055.
[62] P.J. Carl, S.C. Larsen, J. Catal. 196 (2000) 352.